ELSEVIER

Polymer 43 (2002) 2827–2833

polymer

www.elsevier.com/locate/polymer

Liquid–liquid phase separation and crystallization behavior of poly(ethylene terephthalate)/poly(ether imide) blend

Jong Kwan Lee, Woo Suk Choi, Yong Ku Kwon, Kwang Hee Lee*

Center for Advanced Functional Polymers, School of Chemical Science and Engineering, Inha University, Inchon 402-751, South Korea

Received 7 September 2001; received in revised form 10 December 2001; accepted 24 December 2001

Abstract

The liquid–liquid (L–L) phase separation and crystallization behavior of poly(ethylene terephthalate) (PET)/poly(ether imide) (PEI) blend were investigated with optical microscopy, light scattering, and small angle X-ray scattering (SAXS). The thermal analysis showed that the concentration fluctuation between separated phases was controllable by changing the time spent for demixing before crystallization. The L–L phase-separated specimens at 130 °C for various time periods were subjected to a temperature-jump of 180 °C for the isothermal crystallization and then effects of L–L phase separation on crystallization were investigated. The crystal growth rate decreased with increasing L–L phase-separated time (t_s). The slow crystallization for a long t_s implied that the growth path of crystals was highly distorted by the rearrangement of the spinodal domains associated with coarsening. The characteristic morphological parameters at the lamellar level were determined by the correlation function analysis on the SAXS data. The blend had a larger amorphous layer thickness than the pure PET, indicating that PEI molecules in the PET-rich phase were incorporated into the interlamellar regions during crystallization.

Keywords: Liquid–liquid phase separation; Crystallization; Poly(ethylene terephthalate)/poly(ether imide) blend

1. Introduction

The analysis of the morphology of crystalline polymer blends has gained significant momentum over the years. Much attention has been focused on the varied microstructures that result from the crystallization of semicrystalline/amorphous blends [1–4]. One of the important considerations in this case is the location of the amorphous polymeric diluent in the microstructure. The diluent molecules can reside in interspherulitic regions, interfibrillar regions (i.e. between the lamellar stacks), interlamellar regions, or some combination of these, yielding different microstructures. The disposition of the polymeric diluent during crystallization depends on two factors: one is the diffusion of the diluent molecules and the other is the growth rate of the crystal phase [1,3]. If the diffusion is slow and/or the growth rate is fast, the diluent molecules can be trapped between the lamellar, resulting in an interlamellar morphology. When the diffusion is fast and/or the growth rate is slow, the diluent molecules can diffuse out of the lamellar stacks, resulting in an interfibrillar or interspherulitic morphology.

It has been reported that the morphology of crystalline polymer blends is sometimes influenced by a liquid–liquid (L–L) demixing process [5–13]. If the blend has a lower critical solution temperature (LCST) or upper critical solution temperature (UCST) phase diagram, crystallization may proceed simultaneously and compete with L–L phase separation. The two competitive processes may create unique morphological patterns that are not attainable by either process alone. Hashimoto et al. [5,6] studied the role of L–L demixing on the morphology developed by subsequent crystallization in isotactic polypropylene (iPP)/ethylene–propylene copolymer blends. They found that the modulated structure developed by the L–L demixing above the melting point of iPP was conserved during and after crystallization when the crystallization rate was much faster than the rate of mutual diffusion of the constituent polymer molecules but was not conserved when the crystallization rate was sufficiently slow compared with the rate of mutual diffusion. The blend of polycaprolactone (PCL) and polystyrene oligomer (PSO) represented another system that displayed combined crystallization and L–L demixing. Nojima et al. [7] studied the structure development in PCL/PSO blends with various PCL compositions by means of small angle X-ray scattering (SAXS). They reported that the dependence of morphological parameters, such as lamellar thickness and amorphous layer thickness,

* Corresponding author. Tel.: +82-32-862-9507; fax: +82-32-865-5178.
E-mail address: polylee@inha.ac.kr (K.H. Lee).

0032-3861/02/$ - see front matter
PII: S0032-3861(02)00054-X

on the crystallization temperature and PCL composition can be successfully explained in terms of the phase diagram consisting of the binodals and melting point of PCL. Recently, Chen et al. [9,11] studied the morphology of poly(ethylene terephthalate) (PET)/poly(ether imide) (PEI) blends using light scattering (LS) and SAXS techniques. They observed that the PET/PEI blends exhibited combined crystallization and L–L demixing, where a UCST phase diagram was located below the melting point of PET. In contrast to PCL/PSO systems where the PSO-rich phase was characterized by discontinuous droplets, the PET-rich phase was manifested by the highly interconnected domains induced by the spinodal decomposition (SD). They also reported that the L–L demixing exerted a driving force to pull a portion of PEI out of the interlamellar regions to form the exterior PEI-rich domains. The interlamellar regions thus represented the PET-rich phase and had approximately the same thickness irrespective of the overall blend composition.

In this work, a further study has been made of the PET/PEI blend system. We proposed a particular method for the morphology control of the blend. The method involved L–L phase separation to a certain demixing state by SD and subsequent crystallization by annealing the demixing mixture. By using this method, it was found that the concentration fluctuation in the phase-separated domains might be controllable by changing the time spent for demixing before crystallization. The effects of the L–L demixing on the crystallization and the morphology at the lamellar level were also discussed.

2. Experimental

2.1. Materials and sample preparation

PET with the molecular weight of ~23 000 was obtained from SKC Co., Korea. PEI was supplied by General Electric (GE, Ultem 1000) and its number- and weight-average molecular weights were $\bar{M}_n = 12\,000$ and $\bar{M}_w = 30\,000$, respectively. After being dried in a vacuum oven at 150 °C for 24 h, PET and PEI were melt-mixed at 280 °C on a 30 mm corotating twin-screw extruder (Werner Pfleiderer) at 200 rpm. The extrudate was quenched in ice water and was then chopped into pellets. The composition of the blend was 50/50 by weight.

Samples for the thermal analysis and the SAXS study were prepared by compression molding. The pellets were compression-molded between metal plates at 280 °C for 5 min followed by quenching in ice water to obtain an amorphous specimen of ~1 mm thick. Subsequent L–L phase separation was conducted at 130 °C on a Mettler FP82HT hot stage for a certain time (t_s).

2.2. Thermal analysis

The crystallization and the melting behavior were investigated with a Perkin Elmer DSC-7 differential scanning calorimeter (DSC). The samples were heated to 300 °C at a rate of 10 °C/min in a nitrogen atmosphere. Dynamic mechanical measurements were performed with a Polymer Laboratories MKIII dynamic mechanical thermal analyzer (DMTA). DMTA was operated in the dual-cantilever banding mode at a frequency of 1 Hz and a heating rate of 3 °C/min from 25 to 200 °C.

2.3. LS and optical microscopy

A thin-film specimen (ca. 15 μm thick) was prepared by pressing the pellets between two cover glasses at 280 °C. After melt-pressing, the specimen was quenched in ice water and was then annealed onto a hot stage set at 130 °C for the L–L phase separation. After the sample was held at 130 °C for t_s, it was rapidly transferred onto a light scattering hot stage set at a desired crystallization temperature, and the effects of L–L phase separation on crystallization were examined. A polarized He–Ne gas laser of 632.8 nm wavelength was applied to the film specimen. We used the H_v geometry, in which the optical axis of the analyzer was set perpendicular to that of the polarizer.

The L–L phase-separated morphology of the specimen was observed with OM.

2.4. SAXS

All SAXS measurements were performed at room temperature. The X-ray beam was from synchrotron radiation, beam line 4C1 at the Pohang Light Source, Korea. The storage ring was operated at an energy level of 2 GeV. The SAXS employs point-focusing optics with a Si double crystal monochromator followed by a bent cylindrical mirror. The incident beam intensity of 0.149 nm wavelength was monitored by an ionization chamber for the correction of a minor decrease of the primary beam intensity during the measurement. The scattering intensity by thermal fluctuations was subtracted from SAXS profile $I(q)$ by evaluating the slope of a $I(q)q^4$ vs. q^4 plot at wide scattering vector q, where q is $(4\pi/\lambda)\sin(\theta/2)$, λ and θ being the wavelength and scattering angle, respectively [14]. The correction for the smearing effect by the finite cross-section of the incident beam was not necessary for the optics of SAXS with point focusing.

2.5. Method of morphology control

To control the morphology of the blend by SD and crystallization, we employed the thermal history shown in Fig. 1. The melt-quenched starting specimens (cf. process a in the figure) were rapidly heated to a temperature (T_d) above the glass transition temperature (T_g) of the blend and annealed for various lengths of time (t_s) (cf. process b in the figure). The PET/PEI blends have an UCST phase diagram below the melting temperature (T_m). Thus, the system undergoes demixing. The demixing may occur

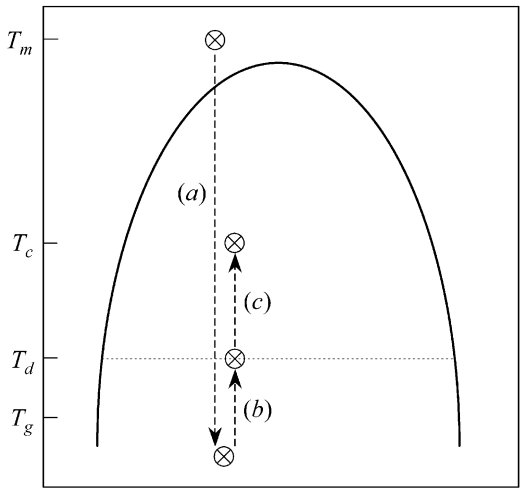

Fig. 1. Schematic diagram showing a thermal history employed in this study for the morphological control by spinodal decomposition and crystallization: T_m, the melting temperature of PET at a given composition; T_c, the crystallization temperature; T_d, the demixing temperature, and T_g, the glass transition temperature of the PET/PEI blend at a given composition.

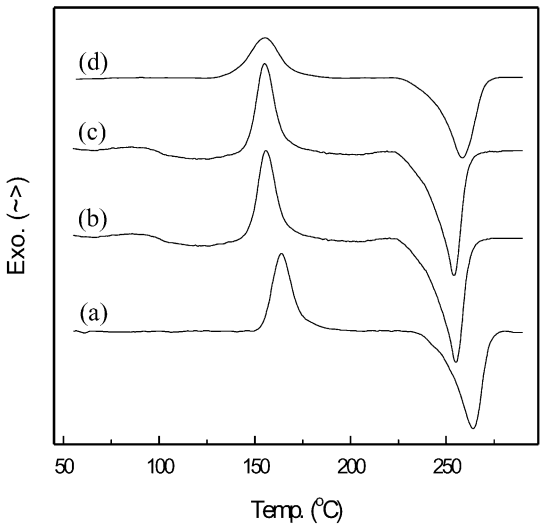

Fig. 2. DSC thermograms of the PET/PEI blend annealed at various temperatures for 10 h after melt-quenching: (a) melt-quenched sample; (b) 130 °C; (c) 135 °C, and (d) 140 °C.

according to SD inside the spinodal phase boundary, as shown by the dotted line in the figure.

An important point to be noted is that at T_d the limited crystallization took place during the annealing. Crystallization rate and SD rate have different temperature dependences. The crystallization rate varies exponentially with temperature in terms of $G \propto \exp(-1/(T_m^0 - T))$ (G and T_m^0 is the crystal growth rate and equilibrium melting temperature, respectively), while the SD rate, characterized by the diffusion coefficient $D = -M(\partial^2 f/\partial \phi^2)$ (M, f, and ϕ are the mobility, free energy density, and volume fraction, respectively) has the temperature dependence of $D \propto |T - T_s|T$ (T_s is the spinodal temperature) [15]. The exponential temperature dependence for crystallization rate is expected to be more sensitive to temperature change. At low T_d, crystallization rate was much slower so that the blend had no chance to undergo considerable crystallization within the time period investigated.

The samples subjected to demixing at T_d for t_s were allowed to crystallize by rapid heating at a given temperature T_c for the isothermal crystallization (cf. process c in the figure). The rapid temperature rise to T_c was produced by inserting the samples into the hot stage set at T_c. At high T_c, the fast crystallization of PET was found to lock in further growth and coarsening of the fluctuations in the demixing process and hence conserve the structure memory in the amorphous state [9].

3. Results and discussion

3.1. L–L phase separation

Fig. 2 shows the DSC thermograms of samples annealed at various temperatures for 10 h after melt-quenching. A conspicuous cold-crystallization peak is clearly observed. An important feature is that the peak area is significantly influenced by the annealing temperature, T_d. The peak areas for the samples annealed at $T_d \leq 135$ °C are almost the same as that for the melt-quenched sample, implying that the samples cannot be thermally crystallized by annealing below 135 °C. However, the sample annealing at 140 °C shows some differences in the cold-crystallization behavior. A large decrease in the cold-crystallization exotherm indicates that the sample is relatively easy to crystallize at 140 °C. We first confine our discussion to the L–L phase separation process without the crystallization. In this study, therefore, the annealing temperature is selected at 130 °C where the L–L phase separation precedes the crystallization.

Fig. 3 shows the DSC thermograms of samples annealed at 130 °C for a period of 0 ~ 20 h. The areas of the cold-crystallization peaks are nearly independent of the annealing time t_s, suggesting that the thermal crystallization is highly restricted during annealing. An interesting feature is the position of the cold-crystallization peaks. As t_s increases, the peak position first shifts to lower temperatures and then moves to higher temperatures. The faster cold-crystallization in the case of $t_s \leq 5$ h may be attributed to the formation of microcrystallites. The small amount of microcrystallites formed during annealing act as the nucleation sites where PET molecules could preferentially crystallize. The crystallization rate is a function of the crystal growth rate G as well as the number of nuclei. When SD precedes crystallization, the modulated morphology will be created before the spherulite growth. Thus, the lamellar crystals grow over a space with a periodic concentration fluctuation and the growth path is a distorted one rather than a straight radial route as encountered in the conventional spherulite growth. If the network structure induced by

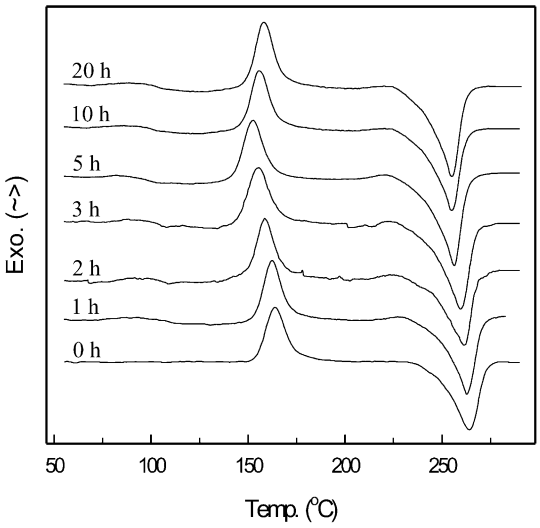

Fig. 3. DSC thermograms of the PET/PEI blend annealed at 130 °C for the indicated t_s.

the L–L phase separation hinders the growth of crystallites (the effects of L–L phase separation on G will be discussed in Fig. 7), the crystallization rate should be decreased. It is seen that the effects of the reduction of the cold-crystallization rate due to the preexisting modulated morphology become more important at the later stage ($t_s > 5$ h). In this system, the fastest cold-crystallization occurs for the sample of $t_s = 5$ h, accordingly. Another phenomenon worth mentioning is the melting behavior of PET. As t_s increases, the melting point is slightly decreased. The L–L phase separation by SD is realized by uphill diffusion; A molecules diffuse into an A-rich phase from a B-rich phase. Thus, PEI molecules in a PET-rich phase may be forced to move into a PEI-rich phase during annealing. As a result, the amount of PEI in the PET-rich phase should be decreased with t_s. Because of the smaller amount of the polymeric diluent, it can be expected that the melting point of PET increase with t_s. Therefore, the decrease in the melting point with t_s suggests that the modulated structure induced by SD changes the habit of the crystal growth, resulting in the development of coarse crystalline structures with a low melting point for PET.

The occurrence of SD during annealing can be demonstrated from the morphology observed by OM. Fig. 4 shows the morphological development of the PET/PEI blend annealed at 130 °C. The blend just after quenching from the melt state is a homogeneous mixture, revealing that the blend is miscible at 280 °C. The homogeneous mixture starts to phase separation by annealing at 130 °C. For the sample of $t_s = 10$ h, a high level of interconnectivity in both phases can be seen, and the phases are regularly spaced. One of the regions (e.g. black region) reflects either the PET- or the PEI-rich region, and the other reflects the region rich in the other component. A two-phase structure with unique periodicity and phase connectivity is one of the hallmarks of SD.

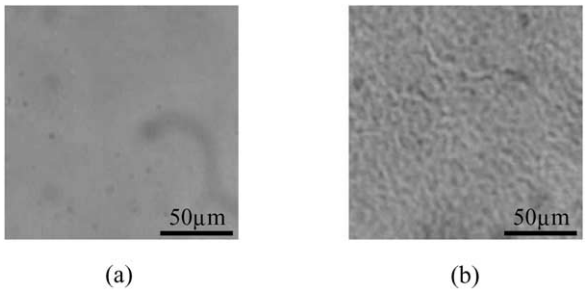

Fig. 4. Optical micrographs of the PET/PEI blend: (a) melt-quenched, and (b) annealed at 130 °C for 10 h.

Dynamic mechanical measurements on the blend samples also provide a supplementary evidence for the L–L phase separation. The temperature dependence of the loss tangent, tan δ of the blend samples annealed at 130 °C for t_s is plotted in Fig. 5. The quenched sample ($t_s = 0$ h) shows a single T_g of intermediate value between the T_gs of the pure component polymers (the T_gs of pure PET and PEI were about 70 and 215 °C, respectively). For the sample of $t_s = 5$ h, the PET transition appears as a shoulder in the broad transition. At longer t_s, two distinct glass transitions are exhibited and the peak positions shift outwardly. The outward shift of the T_gs is interpreted to be due to increased degree of demixing. It is worth noting that a broad range of tan δ peaks depend on the degree of segmental mixing on a molecular scale. The observation of a large broadness of the tan δ peak for the quenched sample suggests that small-scale compositional fluctuations still reside in the melt state even though the PET/PEI blend shows the morphological homogeneity under OM.

3.2. Crystallization

The results in Figs. 4 and 5 show the UCST type phase behavior in the PET/PEI blend. Chen et al. [9] reported that

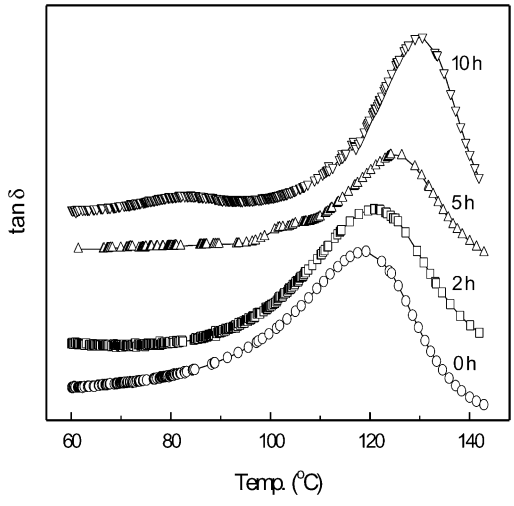

Fig. 5. Temperature dependence of the loss tangent (tan δ) of the PET/PEI blend annealed at 130 °C for the indicated t_s.

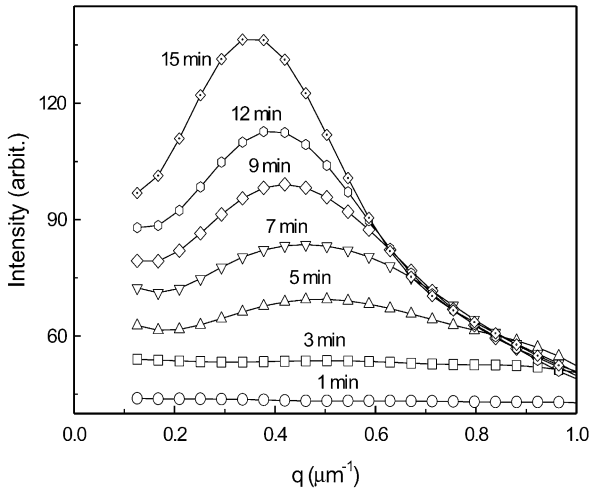

Fig. 6. Time variation of H_v scattering patterns at an azimuthal angle, $\mu = 45°$ during crystallization for the melt-quenched sample.

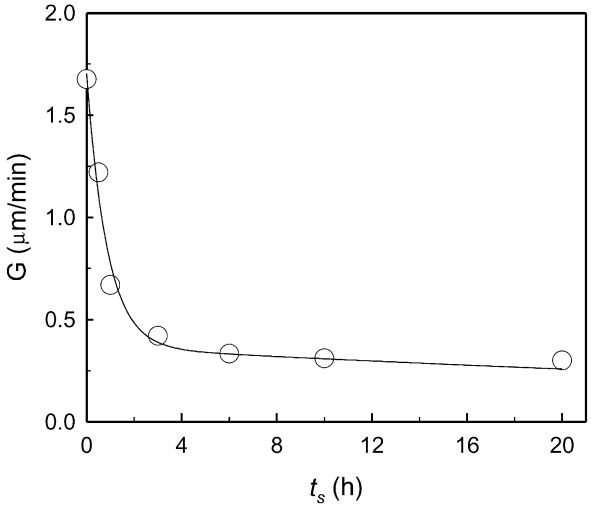

Fig. 7. Change in G with t_s.

above the melting temperature of PET, the single-phase nature was confirmed at all compositions; i.e. the phase-separated structure was not observed under OM. Thus, the UCST should be located below the melting temperature of PET. Such a UCST could be a virtual one but it could not be detected by the cloud point method, which would be disturbed by the crystallization. The virtual UCST may be determined by analyzing the competition of the L–L phase separation with the crystallization using V_v and H_v light scatterings [5,6]. Unfortunately, in the present system, no effective information was obtained from the V_v scattering because of the very small difference in refractive index between the constituent polymers. Effective information was given just at H_v optical alignment.

The H_v scattering profile, the scattered intensity I as a function of scattering angle θ, was measured at appropriate intervals after a temperature jump from 130 °C to the crystallization temperature of 180 °C. Conceptually, it seems plausible that the rapid crystallization of PET at 180 °C is very effective to lock-in further growth of the L–L phase separation. To discuss the crystallization kinetics, it is convenient to employ the H_v scattering profile at an azimuthal angle μ. Fig. 6 shows the time variation of the H_v scattering profile at $\mu = 45°$ during crystallization for the quenched sample. The peak intensity, I_m, increases with time and its position, q_m, shifts to smaller angles. From the position of q_m, the value of the average spherulite radius R_0 can be deduced by [16]

$$R_0 = 4.1/q_m \quad (1)$$

The linear growth rate of spherulite G has a relation expressed by Eq. (2)

$$G = dR_0/dt \quad (2)$$

Therefore, one can determine G from the slope of the time variation of R_0. Fig. 7 shows the change of G for the blend samples crystallized at 180 °C after annealing at 130 °C for t_s. G decreases with t_s, indicating that the crystallization of PET is significantly hindered by the modulated spinodal structure developed during annealing. As the spherulite growth front advances by finding and following the PET-rich domains in the modulated structure, the measured G is dependent on the contour of the PET-rich domains. The spinodal domains are expected to undergo coarsening during SD. Such a long-range structure rearrangement would affect the average shape of contour and subsequently alter the habit of the crystal growth. Therefore, the large decrease in G with t_s strongly suggests that the growth path is highly distorted by the rearrangement of the spinodal domains associated with coarsening. As mentioned earlier, the growth of the concentration fluctuation via SD is achieved by uphill diffusion. The compositions of the two phases may be changing with one phase continued to enrich the PET content (PET-rich phase) while the other continued to enrich the PEI content (PEI-rich phase). As a result, the amount of PEI in the PET-rich phase should be decreased with t_s and the T_g of the PET-rich phase may correspondingly decrease. Because of a smaller degree of impurity and a lower T_g, it can be expected that the crystallization rate of PET for the annealing samples are faster than that for the melt-quenched sample. However, G for the annealing samples are smaller than that for the sample of $t_s = 0$ h. Similar trends were observed at other crystallization temperatures from 150 to 200 °C (data not shown). This implies that the crystallization rate of the PET/PEI blend significantly depends on the change of the long-range structure rearrangement in the modulated spinodal morphology rather than the composition change between separated phases.

3.3. Lamellar morphology

The morphological parameters, including long period (L), crystal thickness (l_c), and amorphous layer thickness (l_a)

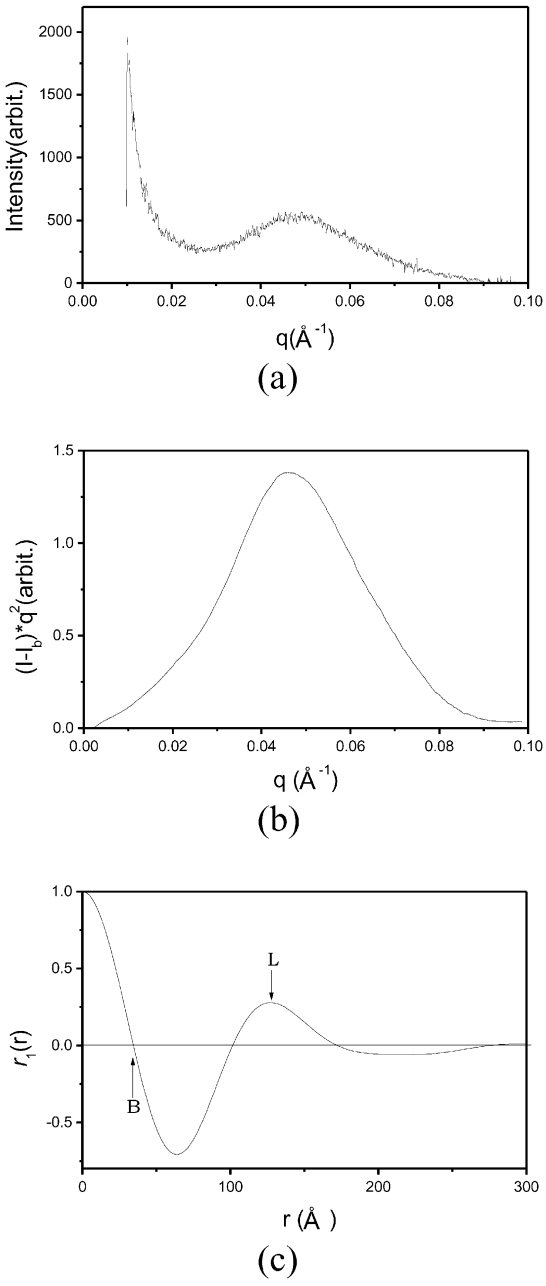

Fig. 8. Illustration of the SAXS data analysis scheme: (a) the typical SAXS pattern for the PET/PEI blend crystallized at 180 °C without annealing; (b) the corresponding Lorentz-corrected plot, and (c) the normalized correlation function.

were determined by SAXS. The raw SAXS data were analyzed via the correlation function approaches [17]. The correlation function is the Fourier transform of the Lorentz corrected SAXS data as given in Eq. (3):

$$\gamma_1(r) = \frac{\int_0^\infty [I - I_b]q^2 \cos(qr)\mathrm{d}q}{\int_0^\infty [I - I_b]q^2 \,\mathrm{d}q} \tag{3}$$

where $\gamma_1(r)$ is the one-dimensional correlation function, I_b is

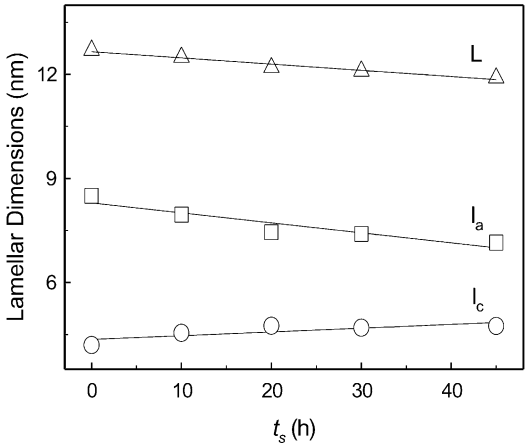

Fig. 9. Plot of lamellar dimensions (L, l_c, and l_a) against t_s for the PET/PEI blend crystallized at 180 °C.

the contribution to scattering from local electron density fluctuations in the amorphous phase (liquid scattering). Because SAXS data are collected in a limited angle range, it must necessarily be extrapolated to both high and low q values before Fourier transformation. The data were extrapolated to low q values (in the beam stop region) assuming a linear $[I - I_b]q^2$ vs. q^2 profile. The extrapolation in the high q region was performed with the aid of the Porod's law. Details of the Porod analysis are reported elsewhere [18,19]. Once the Porod constant and the liquid scattering profile have been estimated, the correlation function can be easily calculated. This calculation is shown in Fig. 8. Plot (a) depicts the raw scattering profile. Plot (b) depicts the corresponding Lorentz-corrected profile and plot (c) depicts the correlation function.

From the correlation function, we estimate L (the first maximum), l_c, and l_a using the following equations [19,20]

$$x_{cl}(1 - x_{cl})L = B \tag{4}$$

$$x_{cl} = l_c/L \tag{5}$$

$$l_a = L - l_c \tag{6}$$

where $x_{cl} = l_c/L$ is the linear crystallinity within the lamellae structure and B is the position of the first intercept of the correlation function with the r axis. Note that Eq. (4) is quadratic in x_{cl} and can be solved to obtain two solutions for x_{cl}. The sum of these two solutions will equal 1, and only one of these solutions corresponds to the lamellar thickness. Chen et. al. [11] studied in detail which one corresponds to l_c or l_a. They reported that the shorter length deduced from the low value of x_{cl} is l_c and the longer length given by $L - l_c$ is l_a.

Fig. 9 shows the plots of L, l_c, and l_a against t_s for the blend samples crystallized at 180 °C. The blend has a much larger l_a than the pure PET (the l_c and l_a values of the pure PET sample crystallized at 180 °C were 58 and 35 Å, respectively [21]), suggesting that PEI in the PET-rich

phase was incorporated into the interlamellar regions during crystallization. One of interesting features is the change in l_a with t_s. In the stage of annealing, PEI molecules in a PET-rich phase may be forced to move into a PEI-rich phase via SD. As a result, the amount of PEI in the PET-rich phase is decreased with t_s and the smaller amount of PEI is correspondingly incorporated into the PET interlamellar regions during crystallization. Therefore, the value of l_a is expected to decrease with t_s as shown in the figure. It is worth noting that l_c of the blend is smaller than the value of 58 Å for the pure PET. Such behavior cannot be explained simply by thermodynamical considerations. If the PEI molecules act as a diluent for PET, we should expect an increase in l_c at a given crystallization temperature because of the decrease in the degree of supercooling. In principle l_c could decrease even in the case of diluent effect through the decrease of quantity ($\sigma_e T_m^0$) [22]:

$$l_c = \frac{2\gamma\sigma_e T_m^0}{\Delta h_f \Delta T} \tag{7}$$

where γ is a constant, σ_e, the surface free energy of folding, T_m^0, the equilibrium melting temperature, Δh_f, the heat of fusion, and ΔT, is the degree of supercooling. The decreased l_c, therefore, would suggest a strong influence of the PEI molecules on σ_e. However, our results do not seem to support such a hypothesis. It is more likely that morphological and kinetic rather than thermodynamic effects are responsible for the l_c depression. The inclusion of the PEI component in intraspherulitic regions during the growth of PET crystals probably cause some kind of hindrance to the development of lamellar crystals, leading to a smaller value of l_c. The increase in l_c with t_s also seemed to attribute to a change in the growth mechanism of the PET/PEI blend as affected by either the composition change of the separated phases or by the change in the structure rearrangement of the modulated spinodal morphology determined by the level of demixing.

4. Conclusions

The crystallization behavior of the PET/PEI blend was influenced by the proceeding L–L phase separation process. Its effects became prominent especially in the later stage of demixing where spinodal domains were rearranged or coarsened. The growth rate of the PET crystals decreased with demixing time, pointing out that the crystal growth path was highly distorted by the spinodal domains. The incorporation of the PEI component in the PET-rich phase was unfavorable for the development of lamellar crystals, leading to a smaller value of crystal thickness. The amorphous layer thickness decreased with demixing time due to the diffusion of the PEI molecules from the PET-rich phase to the PEI-rich phase.

Acknowledgements

This research was supported by the Center for Advanced Functional Polymers. Synchrotron SAXS Experiments at the Pohang Accelerator Laboratory were supported in part by MOST and POSCO.

References

[1] Talibuddin S, Wu L, Runt J, Lin JS. Macromolecules 1996;29:7527.
[2] Chen HL, Li LJ, Lin TL. Macromolecules 1998;31:2255.
[3] Yeh F, Hsiao BS, Chu B, Sauer BB, Flexman EA. J Polym Sci, Polym Phys Ed 1999;37:3115.
[4] Dreezen G, Mischenko N, Koch MHJ, Reynaers H, Groeninckx G. Macromolecules 1999;32:4015.
[5] Inaba N, Sato K, Suzuki S, Hashimoto T. Macromolecules 1986; 19:1690.
[6] Inaba N, Yamada T, Suzuki S, Hashimoto T. Macromolecules 1988;21:407.
[7] Nojima S, Satoh K, Ashida T. Macromolecules 1991;24:942.
[8] Okamoto M, Kotaka T. Polymer 1997;38:1357.
[9] Chen HL, Hwang JC, Yang JM, Wang RC. Polymer 1998;39:6983.
[10] Chen HL, Hwang JC, Wang RC. Polymer 1998;39:6067.
[11] Chen HL, Hsiao BS. Macromolecules 1998;31:6579.
[12] Svoboda P, Keyzlarova L, Soha P, Rybnikar F, Chiba T, Inoue T. Polymer 1999;40:1459.
[13] Bang HJ, Lee JK, Lee KH. J Polym Sci, Polym Phys Ed 2000; 38:2625.
[14] Koberstein J, Morra B, Stein RS. J Appl Crystallogr 1980;13:34.
[15] Hashimoto T, Kumaki J, Kawai H. Macromolecules 1983;16:641.
[16] Stein RS, Rhodes MB. J Appl Phys 1960;31:1873.
[17] Strobl GR, Schneider M. J Polym Sci, Polym Phys Ed 1980;18:1343.
[18] Verma RK, Velikov V, Kander RG, Marand H, Chu B, Hsiao BS. Polymer 1996;37:5357.
[19] Verma R, Marand H, Hsiao B. Macromolecules 1996;29:7767.
[20] Wang W, Schultz JM, Hsiao BS. Macromolecules 1997;30:4544.
[21] Lee JK, Bang HJ, Lee KH. J Polym Sci, Phys Ed. Revised.
[22] Martuscelli E. Polym Engng Sci 1984;24:563.